Supporting Information

A dual-photoelectrode photofuel cell based self-powered aptasensor using a multimeter as a direct visual readout strategy

Meng Zhang, Zhenzhen Zhang, Jie Wei, Zhen Dai, Nan Hao and Kun Wang*

Key Laboratory of Modern Agriculture Equipment and Technology, School of Chemistry and Chemical Engineering, Jiangsu University, Zhenjiang 212013, PR China

Table of Contents

* Corresponding author.

E-mail addresses: wangkun@ujs.edu.cn.

Experimental section

Reagents and chemicals 3

Apparatus 3

Fabrication of the photoanode and photocathode 4

Fabrication of self-powered aptasensor for SMZ 5

Fig. S1 7

Fig. S2 8

Fig. S3 9

Fig. S4 10

Fig. S5 11

Fig. S6 12

Fig. S7 13

Fig. S8 14

Table S1 15

Application in real samples 16

Table S2 16

References 17

Experimental section

Reagents and chemicals

Graphene oxide (GO, 2.0 $mg \cdot mL^{-1}$) solution was obtained from Nanjing XFNANO Materials Tech Co., Ltd. Tetrabutyl titanate (TBOT), sodium borohydride ($NaBH_4$), copper nitrate trihydrate ($Cu(NO_3)_2 \cdot 3H_2O$), hydrazine hydrate ($N_2H_4 \cdot H_2O$ 85%), isopropyl alcohol, 3-aminopropyltriethoxysilane (APTES), sulfamethazine (SMZ), chitosan, glutaraldehyde (GA) solution, albumin from bovine serum (BAS) and Tris (hydroxymethyl) aminomethane (Tris) were purchased from Sinopharm Chemical Reagent Co., Ltd. The SMZ aptamer was purchased from Sangon Biotech Co., Ltd. with the sequences: 5′-NH_2-TTA GCT TAT GCG TTG GCC GGG ATA AGG ATC CAG CCG TTG TAG ATT TGC GTT CTA ACT CTC-3′. Phosphate buffer solution (PBS, 0.1 M, pH 5.0) was employed as the supporting electrolyte, which prepared by mixing of Na_2HPO_4 and NaH_2PO_4. Aptamer and SMZ were respectively dissolved in buffer solution (Tris-HCl, 0.05 M, pH 7.4) to obtain various concentrations of standard samples. All other chemicals were of analytical grade, and the aqueous solutions were prepared with ultrapure water.

Apparatus

The morphology of the samples was characterized by a JEOL JSM-6700 transmission electron microscope (TEM) (Hitachi, Japan). X-ray diffraction (XRD) patterns were recorded by a Bruker D8 diffractometer equipped with high-intensity Cu Kα radiation (Bruker Co., Germany). X-ray photoelectron spectrometry (XPS) analyses were measured using a VG MultiLab 2000 system with a monochromatic Mg-K a source operated at 20 kV. UV-vis diffuse reflectance spectroscopy (UV-vis DRS) was carried out on a UV-2450 spectrophotometer (Shimadzu, Japan). The

digital multimeter (UT15B PRO) was purchased online. The PFC measurements, polarization and electrochemical impedance spectroscopy (EIS) curves were recorded on a CHI 760E electrochemical workstation (Chen Hua Instruments Co., Shanghai, China). The PFC performance was monitored by using a one-compartment cell and 300 W Xenon lamp (PLS-SXE 300C (BF), PerfectLight, Beijing). The V-I curves of the cell were measured with galvanostatic polarization technique. The power output density curves (P-I curves) were presented by plotting the power density vs. the current.

Fabrication of the photoanode and photocathode

B-TiO_2 was prepared according to our previous work.[1] Cu_2O/3DNG composites were synthesized as following. Firstly, the 3DNG was obtained by a one-step hydrothermal process referring to the previously published literature.[2] 0.25 g $Cu(NO_3)_2 \cdot 3H_2O$ was dissolved in 50 mL ultrapure water and then 4 mL $N_2H_4 \cdot H_2O$ (0.5 M) was dropwised into the suspension under magnetical stirring. The solid products were separated by centrifugation and washed several times, kept in vacuum oven at 60 °C for 12 h to obtain Cu_2O nanospheres. Afterwards, 0.1 g of the as-prepared Cu_2O was dispersed into the mixture of 0.1 mL APTES and 10 mL isopropyl alcohol with constant stirring for 24 h. After being washed by ultrapure water and absolute ethanol, positively charged surface-functionalized Cu_2O nanospheres were collected and then redissolved in 50 mL ultrapure water including 20 mL of nitrogen-doped graphene aqueous solution (1 $mg \cdot mL^{-1}$). The above suspension was stirred for 4 h at room temperature, followed by washing with water and ethanol several times,

and dried at 60 °C in a vacuum oven for 12 h. Finally, the Cu_2O/3DNG composites were obtained.

To fabricate the modified photoanode and photocathode, firstly, the indium tin oxide (ITO) glass was pretreated in ethanol by sonication, and dried under an infrared lamp for subsequent use. B-TiO_2 and Cu_2O/3DNG suspension (2 mg mL^{-1}) were respectively prepared with N,N-dimethylformamide (DMF). Then, 20 μL B-TiO_2 and Cu_2O/3DNG dispersion was dripped on the as-prepared ITO (with an exposed geometric area of 0.09π cm^2) and dried under the infrared lamp. The obtained modified electrodes B-TiO_2/ITO and Cu_2O/3DNG/ITO were employed as the photoanode and photocathode, respectively.

Fabrication of self-powered aptasensor for SMZ

As shown in Scheme 1C, the self-powered aptasensor for SMZ was constructed. First of all, chitosan solution (10 μL 0.1%) was coated on the surface of photoanode B-TiO_2/ITO and dried under the infrared lamp. As the cross-linking agent, glutaraldehyde (GA) solution (20 μL 2.5%) was dropped onto the above electrode for 1 h at room temperature, and then PBS was used to rinse the excess GA gently. Subsequently, the electrode was covered by 20 μL aminated SMZ aptamer solution (3 μM), and incubated for 12 h in the refrigerator, followed by washing with PBS slowly to remove the redundant unbound aptamer. In order to block the nonspecific binding sites, 20 μL 3% bovine serum albumin (BSA) was coated on the photoanode for half an hour, and washed by PBS softly. Finally, the construction of the self-powered aptasensor was facilely done by combining the as-prepared photoanode aptamer/B-

TiO_2/ITO and photocathode Cu_2O/3DNG/ITO in a single-chamber quartz cell with PBS (0.1 M, 20 mL) as electrolyte, and Xenon lamp was used to illuminate the electrodes vertically. The multimeter connected with two photoelectrodes to display voltages directly.

To perform the recognition between aptamer and SMZ, the photoanode aptamer/B-TiO_2/ITO was incubated with 20 μL SMZ standard solution of different concentrations for 40 min at 37 °C, and flushed with PBS thoroughly. In the end, the voltage output of the PFC was tested by the multimeter.

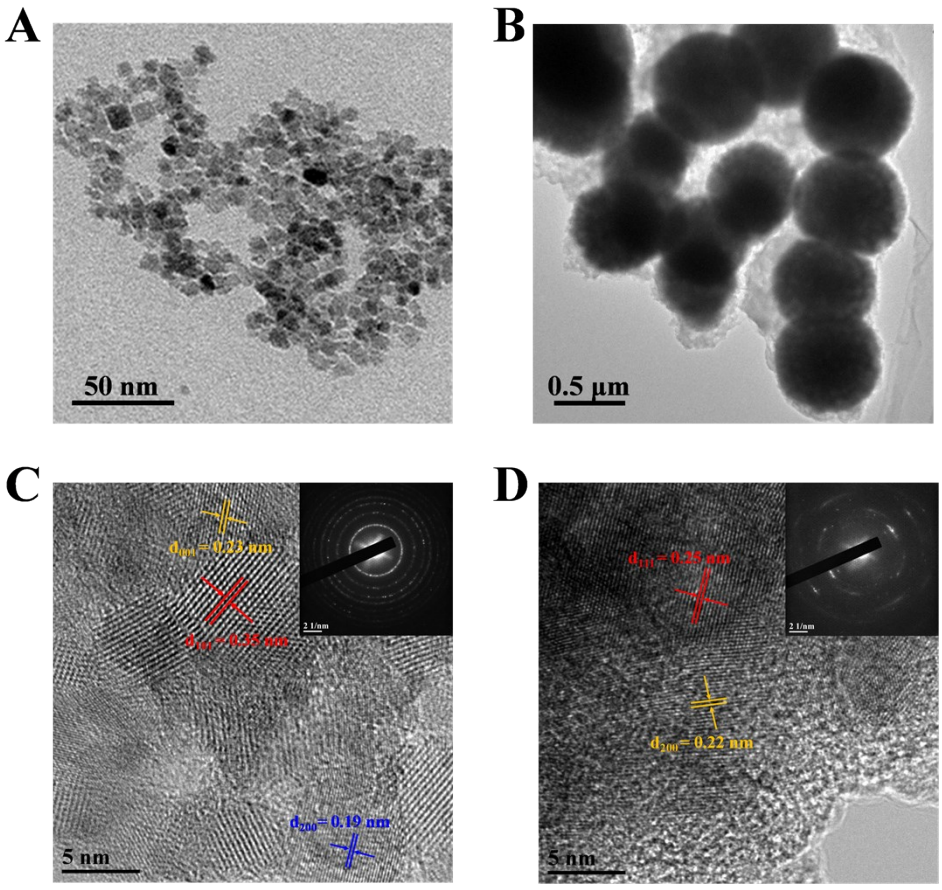

Fig. S1. TEM images of (A) B-TiO_2 and (B) Cu_2O/3DNG; HRTEM images of (C) B-TiO_2 and (D) Cu_2O/3DNG; insets: SAED patterns.

The high-resolution TEM (HRTEM) image (Fig. S1C) showed that B-TiO_2 was well crystallized, and the d-spacings of 0.19 nm, 0.23 nm and 0.35 nm corresponding to the (200), (001) and (101) crystal lattices of anatase TiO_2 were clearly observed. And the selected area electron diffraction (SAED) of B-TiO_2 further confirmed its polycrystalline nature. A HRTEM image taken from the selected area of Cu_2O/3DNG was shown in Fig. S1D. The observed interplanar spacing of 0.22 nm and 0.25 nm corresponds to (200) an (111) lattice plane of Cu_2O, respectively. The inset of SAED pattern also demonstrated polycrystallinity of Cu_2O/3DNG.

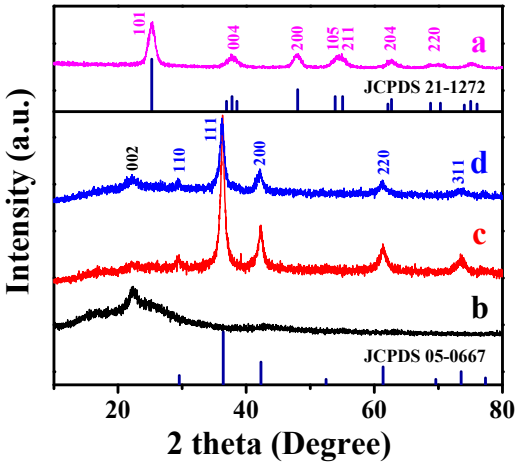

Fig. S2. XRD patterns of B-TiO_2 (a), 3DNG (b) Cu_2O (c) and Cu_2O/3DNG (d).

XRD patterns are depicted in Fig. S2 to study the crystal structures. In the pattern of B-TiO_2 (curve a) from previous work, all the diffraction peaks were indexed to the JCPDS 21-1272.[1] For 3DNG (curve b), a broad peak at about 22.5° corresponded to the characteristic (002) reflection of the hexagonal structure of nitrogen-doped graphene.[3] The pristine Cu_2O (curve c) displayed characteristic peaks with 2θ values at 29.4°, 36.2°, 42.1°, 61.3° and 73.6°, which were attributed to the (110), (111), (200), (220) and (311) planes of Cu_2O, respectively.[4] The as-synthesized Cu_2O/3DNG (curve d) had diffraction peaks of both Cu_2O and 3DNG, indicating that Cu_2O spheres were successfully loaded on 3DNG.

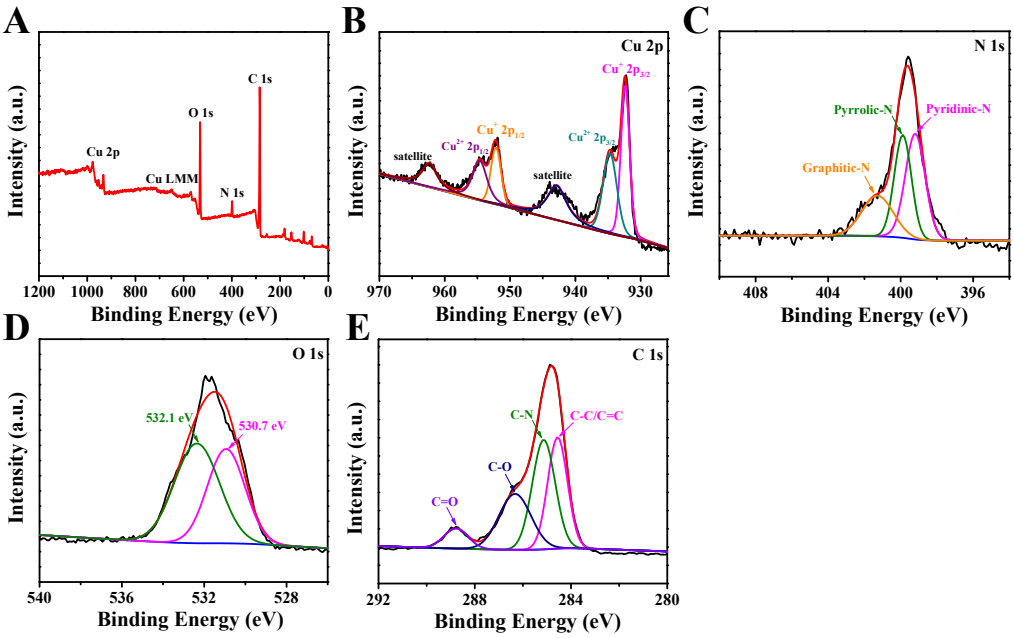

Fig. S3. (A) XPS survey spectra of Cu_2O/3DNG. The high-resolution (B) Cu 2p, (C) N 1s, (D) O 1s and (E) C 1s spectrum of Cu_2O/3DNG.

XPS was utilized to characterize the chemical binding and elemental composition of Cu_2O/3DNG. The full survey XPS spectra (Fig. S3A) revealed the coexistence of elements Cu, O, C and N. Fig. S3B shows the Cu 2p high resolution spectrum, where the two peaks located at 952.1 and 932.4 eV could be assigned to Cu $2p_{1/2}$ and Cu $2p_{3/2}$ of Cu^+.[5] Meanwhile, there are two small peaks at 954.6 and 934.7 eV and two shake-up satellite peaks, which were attested to characteristic peaks of a CuO phase.[5] This phenomenon might be attributed to the fact that some Cu^+ was oxidized to Cu^{2+} due to the long exposure to the air, however, the XRD patterns showed that the products still remain in the pure Cu_2O phase.[6] The N 1s narrow spectrum (Fig. S3C) could be divided into three peaks at 401.3, 399.9 and 399.1 eV, corresponding to graphitic-N, pyrrolic-N and pyridinic-N, respectively.[7,8] In the spectrum of O 1s (Fig. S3D), two peaks at 532.1 and 530.7 eV were originated from

adsorbed oxygen (surface hydroxyl group or the adsorbed H_2O) and the lattice oxygen of Cu_2O.[3] Furthermore, the C 1s spectra (Fig. S3E) were composed of four peaks at 288.7, 286.3, 285.1 and 284.5 eV that were associated with the C=O, C–O, C–N and C–C/C=C groups.[9] The existence of C–N further proved the N-doping of the carbon framework of graphene. The XPS analysis of B-TiO_2 was explained in our previous work.[1]

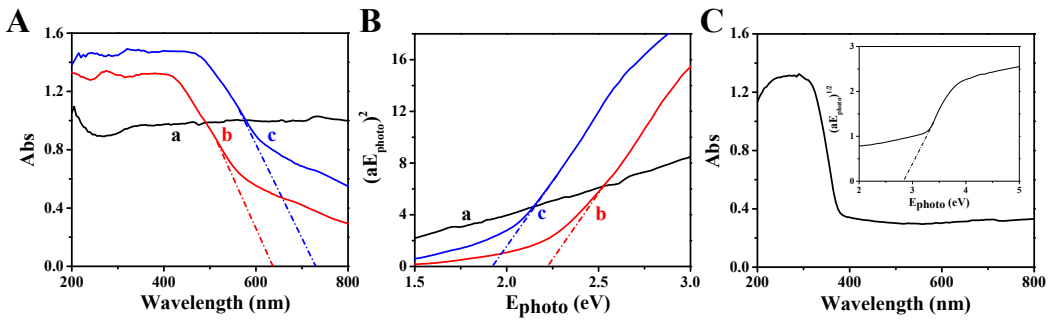

Fig. S4. (A) UV–vis DRS and (B) plots of $(Ahυ)^2$ versus hυ of 3DNG (a), Cu_2O (b) and Cu_2O/3DNG (c), (C) UV–vis DRS of B-TiO_2, inset: plots of $(Ahυ)^{1/2}$ versus hυ of B-TiO_2.

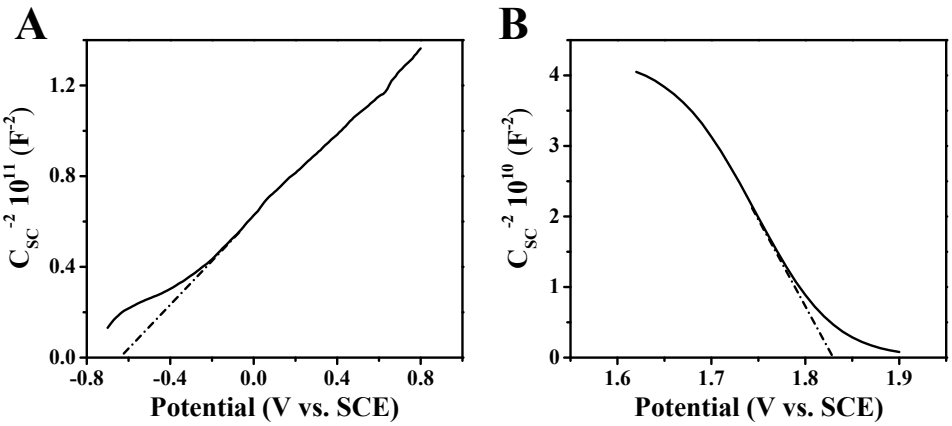

Fig. S5. The Mott-Schottky plots of (A) B-TiO_2/ITO and (B) Cu_2O/3DNG.

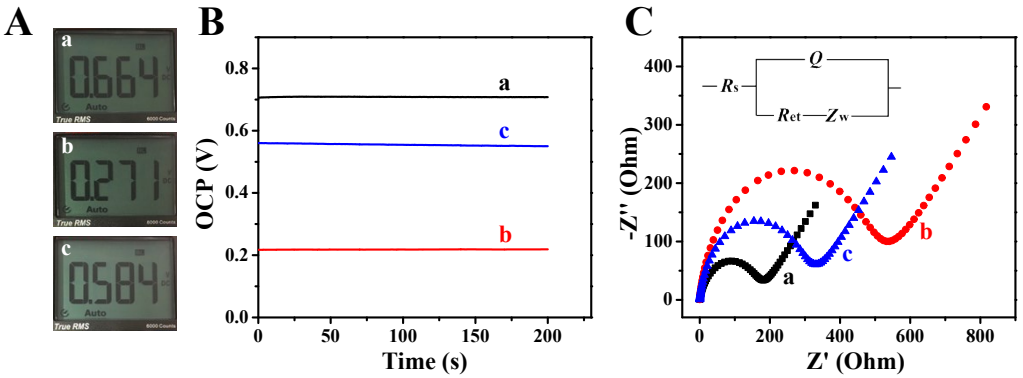

Fig. S6. (A) digital photos of multimeter, (B) OCP and (C) EIS spectra of PFCs using Cu_2O/3DNG as a photocathode with different modified photoanodes of B-TiO_2/ITO (a), aptamer/ B-TiO_2/ITO (b) and SMZ/aptamer/B-TiO_2/ITO (c). The inset of Fig. S6C: equivalent circuit of EIS, where R_{et}, Z_w, R_s, and Q represent electron transfer resistance, Warburg impedance, electrolyte solution resistance, and constant phase elements, respectively.

To further explore the interfacial electron transfer performance of different modified electrodes, EIS analysis was performed (Fig. S6C). The electron transfer resistance (R_{et}) increased from 184.3 (curve a) to 536.6 Ω (curve b) because of the steric hindrance effect of SMZ aptamer, which demonstrated that NH_2-aptamers were successfully immobilized on the photoanode B-TiO_2/ITO via covalent bonding. When SMZ was incubated with aptamers, the R_{et} of photoanode decreased to 330.5 Ω due to the formation of SMZ-aptamer complex, which changed the structure of the aptamers. This change made the electron of $[Fe(CN)_6]^{3-/4-}$ transfer to the electrode surface more freely, resulting in a decrease of R_{et}.[10-12] These results corresponded to PFC output voltages.

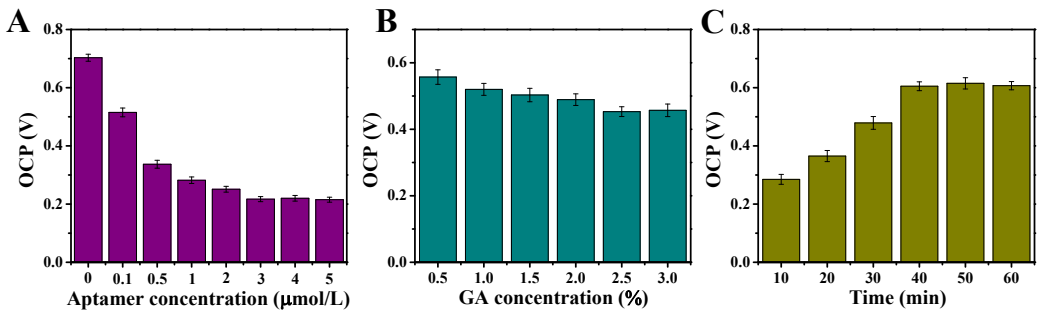

Fig. S7. Effect of (A) aptamer concentration, (B) GA concentration and (C) incubation time of SMZ on OCP of B-TiO_2/ITO.

Aptamer concentration, crosslinking agent GA concentration and the incubation time of SMZ had a significant effect on the properties of the proposed self-powered aptasensor. As displayed in Fig. S7A, the OCP responses decreased with increasing aptamer concentration from 0 to 5.0 μM, and reached a plateau at 3 μM. Therefore, saturation occurred at 3 μM which was selected as the optimized aptamer concentration. Fig. S7B presented that the OCP value gradually decreased and arrived a bottleneck when the GA concentration was 2.5 %, which was the optimized crosslinking agent concentration. In Fig. S7C, at the beginning, the OCP value changed with the incubation time of SMZ, then OCP remained almost unchanged after 40 min. Thus, 40 min was the optimized incubation time.

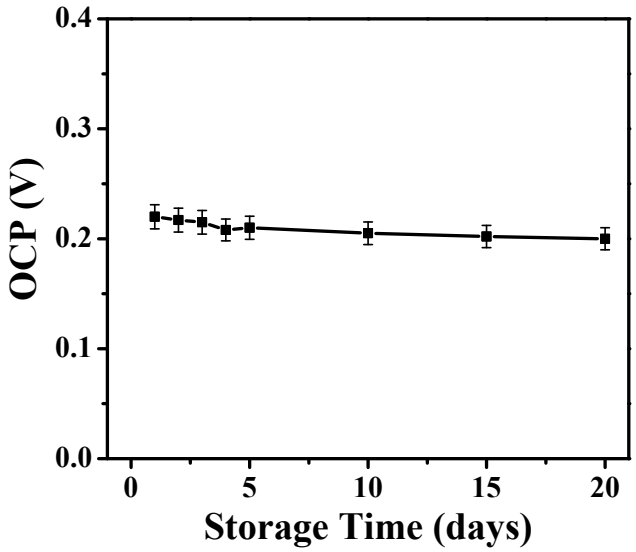

Fig. S8. The repeatability measurement of the as-fabricated self-powered aptasensor.

Table S1 Comparison of the analytical performances of several methods for determination of SMZ.

Method	Material	Detection limit (ng/mL)	Liner range (ng/mL)	Real samples	Reference
Mass spectrometry	/	7.9	1-500	pig body fluids	[13]
Fluorescence immunoassay	AgNCs	0.05	0.14-71.71	water/milk/swine urine	[14]
Enzyme-linked aptamer assay	/	0.05	0.1-10	chicken	[15]
Electrochemical aptasensor	MWCNTs@GONRs	5.2×10^{-3}	0.01-50	chicken	[16]
Lateral flow immunoassay	magnetic nanobeads	0.026	0.033-33	milk	[17]
Immunochromatographic strip	colloidal gold	2	0.01-1000	meat/egg	[18]
PFC aptasensor	B-TiO_2, Cu_2O/3DNG	0.33×10^{-3}	0.001-100	milk	this work

Application in real samples

To further attest the feasibility of this strategy, the aptasensor was employed to complete the detection for SMZ in real food samples of milk. The milk was purchased from the local supermarket (Zhenjiang,PR China). Firstly, the milk was pretreated by centrifuge for 30 min at 15,000 rpm and then the suspensions were diluted 10 times with buffer solution (Tris-HCl, 0.05 M, pH 7.4). Thereafter, SMZ were spiked into the diluted milk via standard addition method to obtain various SMZ standard solutions of 0.01, 0.1, 1 and 10 ng mL^{-1}. As illustrated in Table S2, the recoveries were 97.3 ~ 113.0 % with the RSD of 1.7 ~ 4.1 % according to the same test procedure above, validating the promising potential of the PFC self-powered sensor for SMZ detection in practical application.

Table S2 Analytical results of SMZ in milk samples using the self-powered aptasensor (n = 3).

Sample	Spiked (ng/mL)	Found (ng/mL)	Recovery (%)	RSD (%)
1	0	0	/	/
2	0.01	0.0113	113.0	2.5
3	0.1	0.0973	97.3	3.2
4	1	0.9908	99.08	1.7
5	10	10.24	102.4	4.1

References

1. M. Zhang, Z. Zhang, Y. Xu, Z. Wen, C. Ding, Y. Guo and K. Wang, *Biosens. Bioelectron.*, 2020, **156**, 112135.
2. J. Li, J. Jiang, H. Feng, Z. Xu, S. Tang, P. Deng and D. Qian, *RSC Adv.*, 2016, **6**, 31565-31573.
3. J. Li, J. Jiang, Z. Xu, M. Liu, S. Tang, C. Yang and D. Qian, *Sensor. Actuat. B: Chem.*, 2018, **260**, 529-540.
4. T. Gan, Z. Wang, Z. Shi, D. Zheng, J. Sun and Y. Liu, *Biosens. Bioelectron.*, 2018, **112**, 23-30.
5. F. N. I. Sari, C. Lin and J.-M. Ting, *Chem. Eng. J.*, 2019, **368**, 784-794.
6. Y. Zhang, X. Wang, L. Zeng, S. Song and D. Liu, *Dalton Trans.*, 2012, **41**, 4316-4319.
7. H. Ning, Q. Mao, W. Wang, Z. Yang, X. Wang, Q. Zhao, Y. Song and M. Wu, *J. Alloys Compd.*, 2019, **785**, 7-12.
8. J. Li, J. Jiang, Z. Xu, M. Liu, S. Tang, C. Yang and D. Qian, *Electrochim. Acta*, 2018, **260**, 526-535.
9. B. M. Abu-Zied, M. A. Hussein, A. Khan and A. M. Asiri, *Mater. Chem. Phys.*, 2018, **213**, 168-176.
10. Z. Y. Lin, H. M. Huang, Y. X. Xu, X. Y. Gao, B. Qiu, X. Chen and G. N. Chen, *Talanta*, 2013, **103**, 371-374.
11. S. Eissa, A. Ng, M. Siaj and M. Zourob, *Anal. Chem.*, 2014, **86**, 7551-7557.
12. M. Labib, A. S. Zamay, D. Muharemagic, A. V. Chechik, J. C. Bell and M. V.

Berezoyski, *Anal. Chem.*, 2012, **84**, 1813-1816.

13. S. Suraritdechachai, C. Charoenpakdee, I. Young, S. Maher, T. Vilaivan and T. Praneenararat, *J. Agric. Food Chem.*, 2019, **67**, 3055-3061.

14. N. Zhu, Y. Zhu, J. Wang, E. Gyimah, X. Hu and Z. Zhang, *Talanta*, 2019, **199**, 72-79.

15. T. Le, Q. Sun, Y. Xie, L. Shu, J. Liu, J. Xu, J. Xiong and X. Cao, *Food Anal. Method.*, 2018, **11**, 2778-2787.

16. B. He, M. Li and M. Li, *Mikrochim. Acta*, 2020, **187**, 274.

17. B. L. Fang, S. Hu, C. Wang, M. F. Yuan, Z. Huang, K. Y. Xing, D. F. Liu, J. Peng and W. H. Lai, *Food Control*, 2019, **98**, 268-273.

18. W. B. Shim, J. S. Kim, M. G. Kim and D. H. Chung, *J. Food Sci.*, 2013, **78**, M1575-M1581.